Chapter 2
Characterization of High Frequency Pulse Loading on Fatigue of Metals

Paul A. Lara, Hugh A. Bruck, and Edda C. Müller

Abstract Aluminum materials of various grades are utilized across many industries, spanning from the cycling, automotive, aerospace, and the marine industry. In the marine grade, aluminum materials are utilized to construct entire vessels of various lengths or portions of them by taking advantage of the lower weight characteristics of the materials and impact on stability of the structures. In particular, 5xxx series aluminum materials are relied on by the marine industry for these purposes, taking advantage of the ability of these series to resist marine corrosive environments. However, during its lifetime, a marine vessel will experience a multitude of variable amplitude loading conditions, with occasional overloads and underloads depending on the operation and environmental conditions. In some cases, these overloads/underloads can result in the failure of the structures by reaching its ultimate capacity, but in other instances, they can systematically affect the growth rate of localized cracks. Existing models, like the Wheeler, Willenborg, plus variations of these, have been utilized to predict the crack growth behavior with varying degrees of success. We created an experimental matrix to explore the effects of overload/underload combinations on fatigue crack growth in 5xxx aluminum. Both visual inspection of crack tip location and digital image correlation (DIC) characterization of the crack tip deformation fields were used to characterize the crack growth in center crack tension (CCT) panel specimens. DIC also enabled additional analysis of strain fields to elucidate on the conditions responsible for change in the crack growth behavior. This chapter outlines some of the ongoing results of this work, which built on past experimental work conducted. Future phases of this work will utilize this data to develop new models for fatigue crack growth, and application of multiple pulses sequences.

Keywords Fatigue crack growth · High frequency pulse · Overloads/underloads · Plastic zone · Crack kinking

2.1 Introduction

Embedded high frequency (HF) signal effects derived from wave impacts on ships can affect failure mechanisms on the structures and have an adverse impact on the fatigue life of the vessel. While operating in a sea environment, ship structures can be subject to many operational loads (wind, pressure, temperature, etc.), one of which is the structural effects derived from the surrounding sea environment. Typically, the wave environment applies an ordinary wave component which drives the primary bending stress of the vessel, along with a more stochastically driven element that manifest itself as wave impacts. This dynamic wave impacts results in a high frequency vibratory response signals load applied to ship structures. The vibratory nature of these high frequency responses makes the design of structures increasingly complex in nature due to their uncertainty; designers and naval design rule societies have relied on methods such as safety factors and/or margins of safety to account for its effects. A typical wave impact on a naval structure imparts a time-dependent pulse load that exhibits a higher frequency logarithmic decaying sinusoidal response when measured via experimental means and captured utilizing

P. A. Lara
Naval Surface Warfare Center, Carderock Division, West Bethesda, MD, USA
e-mail: lara@umd.edu

H. A. Bruck (✉)
Mechanical Engineering Department, University of Maryland, College Park, MD, USA
e-mail: bruck@eng.umd.edu

E. C. Müller
Düsseldorf University of Applied Science, Düsseldorf, Germany
e-mail: edda.mueller@study.hs-duesseldorf.de

data acquisition systems. The figure below displays one of these signals, where the measured signal can be decomposed into its different components by applying filtering techniques.

Under the current practices, the peaks of these responses are utilized to compare to the quasi-static design stresses as well as evaluate the fatigue life of the structures either under constant or variable amplitude experimentation. Figure 2.1 below displays this kind of behavior, where underloads and underloads affect the crack growth rate behavior of material under a simplified signal approach [1].

But there are additional higher frequency characteristics to these high frequency signals that are not currently taken into consideration. Existing academic research has been centered on capturing a simplified sinusoidal response associated with this slamming event and embedded high frequency response but has not addressed logarithmic decay, signal frequency, or frequency of occurrence. Work by Sumi et al. has centered on more complex signals, where bounding functions were used to predict crack growth behavior [2], and the results show an influence of crack length predictions based on utilizing these bounding functions.

All these factors have associated uncertainty and impact fatigue life and failure mechanisms exhibited by ship structures; work by researchers such as Fricke et al. has shown damage variation related to the amplitude of high frequency signals [3]. These high frequency effects can cause retardation of crack growth, and foundational models such as Wheler [4] and Willenborg [5] were developed to capture the overall effects of these overloads and underloads. Follow-on work was carried out to gain better understanding of the conditions present, as shown in Fig. 2.2, where the crack growth effects within the overload plastic zone boundary exhibits a variable crack growth rate behavior instead of constant crack growth retardation effect.
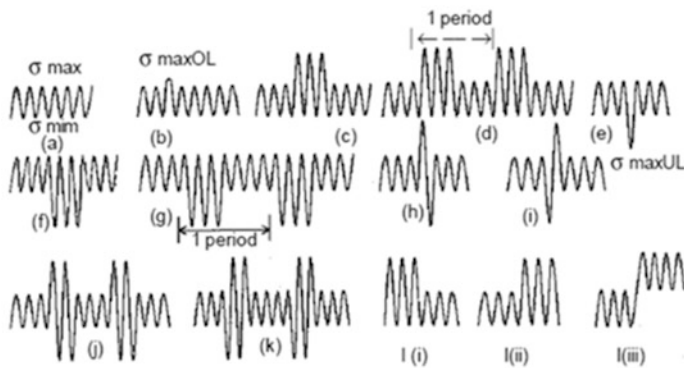
(a) CAL; typical VAL sequences; (b) single OL; (c) block of OL; (d) period blocks of OL; (e) single UL; (f) block of UL; (g) period blocks of UL; (h) single OL-UL; (i) single UL-OL; (j) periodic OL-UL blocks; (k) periodic UL-OL blocks; and (l) two-level block loading — l(i) high-low; l(ii) low-high; and l(iii) both maximum and minimum load
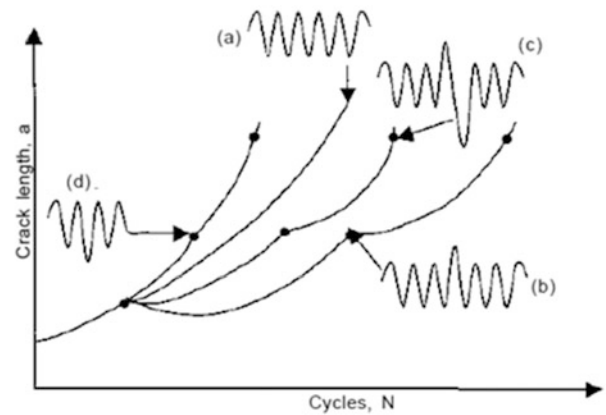
Figure 3 Transient effects on crack growth produced by (a) CAL; (b) single overload; (c) tensile-compressive overload sequence; and (d) single underload
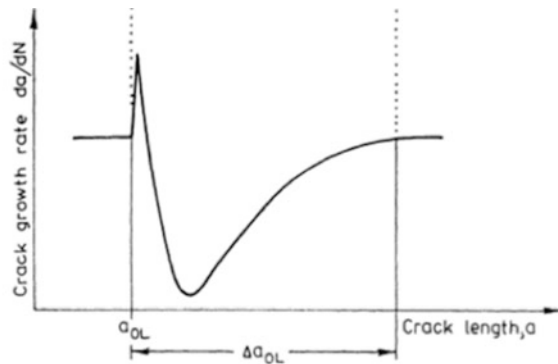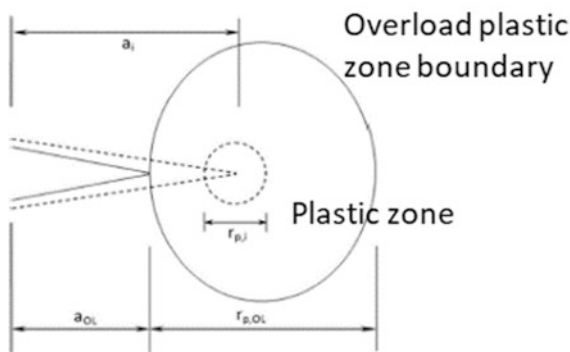
Fig. 2.1 Load sequencing [2]

Fig. 2.2 Plastic zone model and retardation effects, left [6], right [7]

Existing literature gaps are: a deeper understanding of resulting fundamental inelastic aluminum behavior for center crack tension (CCT) specimens due to HF pulses elucidate the plastic zone behavior and resulting material failure modes by leveraging full strain field displacement measurements from digital image correlation (DIC) and develop failure models that accounts for observed material failure behavior due to HF pulses and overall fatigue life response. In the future, the foundational findings of this research can then be leveraged in investigative efforts to develop analytical models addressing heat-affected zones, provide underpinnings for high fidelity numerical modelling, eventually providing broader toolsets to designers that can be used to reduce the dependency on safety factors and introduce more rigorous failure mechanism design criterion.

The work outlined here builds on previous work carried out by the authors; it summarizes some previous work, presents new findings, highlights future efforts, and in the end has an overall objective to gather fundamental understanding of the effects of this high frequency loading on Aluminum 5xxx material, accounting for some of the signal's characteristics, and through an experimental evaluation assesses its impact on the local failure mechanism and life cycle models.

2.2   Description of Experiments

This section outlines a summary of the experimental setup; the work builds from and complements existing work developed by Hart and Bruck [8], where the investigators looked at failure of aluminum 5052-H32, the applications of composite patches to aluminum, and the effects of crack growth. Whereas their work centered on the utilization of a composite laminate to mitigate crack growth on ultimate failure, this work looks at the effects of crack growth based on loading condition. Figure 2.3 below displays the aluminum material properties that Hart and Bruck obtained utilizing ATSM 8 [9] and American Society for Testing and Materials (ASTM) E466 [10], as well as the layout of their center crack panel specimens. The Modulus listed for the material is 70.9 MPa, the yield at 2% offset is 116 MPa, and the parameters α and n at 9.9 and 0.22, respectively.

Initial experiments were carried out on this setup for this work, utilizing a two-post Bose ElectroForce frame which has the capacity of applying loadings up to 100 Hz and 3000 N. This device has a built-in displacement meter with errors less than 5 μm, and it has a block waveform generation software that allows for the implementation of unique load signals. Fast Fourier Transforms methods were utilized to ensure that the programmed signal and the applied signals displayed the required frequencies. But the initial results indicated that there was an imbalance of crack growth between the left and right cracks growing from the notch during fatigue loading, the reason as traced to the use of mechanical wedge friction grips. It is important to mention that the experiments by Hart and Bruck utilized a 4-post MTS servo hydraulic grip setup
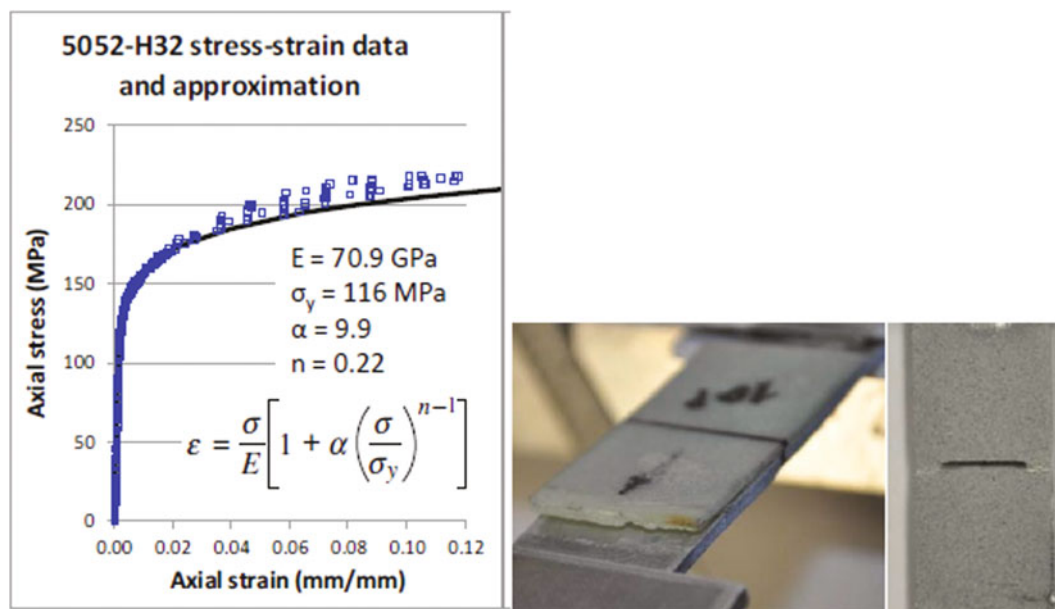

Fig. 2.3 5052-H32 material properties and specimen failure [5]
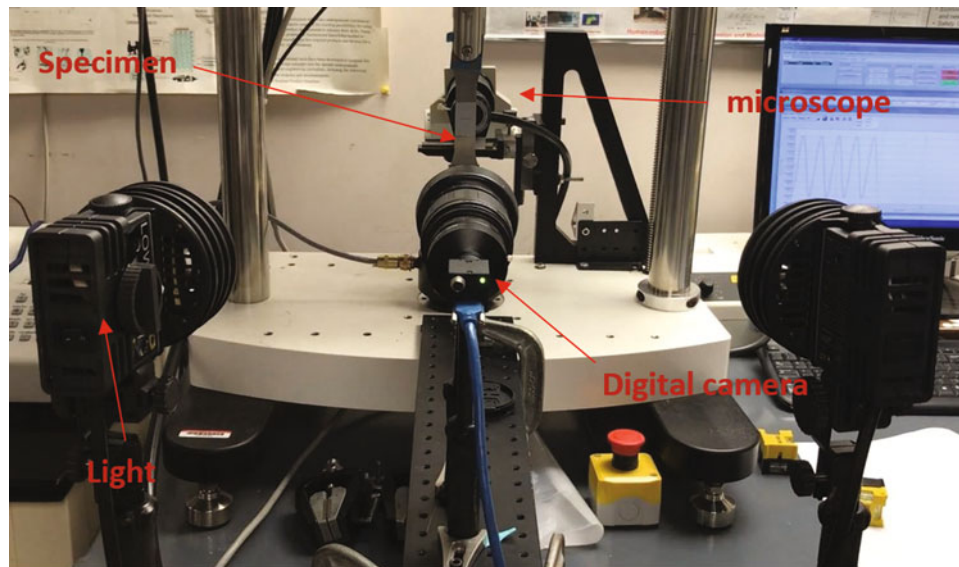
Fig. 2.4 Experiment setup

since they were interested in the ultimate loading capacity. To address this crack asymmetry from loading imbalance, a specimen configuration was developed, and it is an amalgamation of several ASTM methods; this was conducted to address the significant asymmetry observed with crack growth, as previously described. ASTM E8 [9] guidance was utilized to develop the specimen tapers toward test region, while ASTM E647 [11] middle tension specimen configuration was utilized to size the center notch and test region, maintaining the configuration carried out by Hart and Bruck. Since a clevis pin was utilized, ASTM E338 [12] was utilized to develop end reinforcements and alignment tabs for the end pin connections to ensure the failure would not occur in or adjacent to the clevis pin area.

Electrical discharge machining (EDM) techniques were utilized to manufacture the specimens, providing a high level of accuracy for the component geometry, since it was also critical to ensure alignment of end pins and size and location of center notch. The material for the specimen is marine grade aluminum 5052-H32, with a nominal thickness of 2.29 mm (0.09in). Figure 2.4 shows how the clevis pins were utilized in the loading train and end adaptors were used to interface with the Bose frame and to help with specimen load alignment; the Universal Grip LLC. components were utilized for this setup: Adapter - Male Bolt 5/8″–18 w/1″ length, Universal Joint Adapter; in addition, Mark-10 G1090 high-capacity clevis grip (pair) were utilized. The load capacity of the members was at a minimal load of 9KN, hence far exceeding the capacity of the Bose equipment of 3KN, and ensuring no failure could be accidentally induced to the Bose fixture from a failure of the adapters under load.

The experimental setup consisted of several components' setup to provide dual measurements: one was to observe/capture the crack growth on the back of the specimens using a microscope and another to capture digital image correlation information for the future extraction of surface strain measurements. Figure 2.4 details the setup utilized for these experiments.

In the back face of the specimens, an optics zoom inspection microscope head by Edmunds Optics was used along with a Dolan-Jenner MI-150 fiber optic illuminator with a fiber optic ring light accessory. This was utilized to capture the crack growth on the back of the specimen. The setup was connected with a rack and pinion positioning system, which allowed movement of the microscope along three axes to allow consistent positioning of the microscope in different locations to capture crack growth. The microscope was able to visualize square areas of 0.5 mm on each side. Several digital pictures were taken on each crack emanating from each notch, which overlapped, and then were stitched together to form an overall view of the crack of the specimen.

In the front face of the specimen, a Point Gray Flea FL3-U3-88S2C-C digital camera attached to a Tamron 28–80 mm f/3.5–22 lens and an adapter was used to capture static pictures of the surface of the specimen. In addition, two 250 Watts halogen Lowel Pro Lights were utilized to provide lighting to the specimen. The lights set on flood (wide) mode were not directly aimed at the specimens, but instead aimed at locations adjacent to the mid-point of the specimen, and focused as to provide evenly dispersed light flooding on the specimen. Digital image correlation (DIC) was utilized on the front face of the specimen to capture field surface strains [13]; in order to capture these images, the area was prepped to generate distinct patterns that can be captured with a Point Grey FlyCap 2 V2.11.3 and processed utilizing VIC-2D Ver6.0.6 by Correlated Solutions (Lexington, SC).

Figure 2.5 shows the typical DIC pattern applied; the generation of this pattern is achieved by first applying a coat of flat white paint as the background, and the black speckle patterns rely on lightweight particles that slowly settle over the specimen. Best practices developed throughout several references were utilized to obtain acceptable DIC results, once such body of work was developed by the international digital image correlation society [14].

2.3 Test Matrix for HF Pulse Loading Conditions

In order to explore the variability of the high frequency pulses, a couple of items were developed: the first was a consistent process/protocol that was repeatable across experiments, and the second was an experimental matrix that varied certain parameters to determine their influence on the response. Figure 2.6 below outlines the top-level experimental process utilized.

Specimen preparation was the initial step in the configuration; the back of the specimens that faced the microscope was polished to a mirror-type finish; this aided in the identification of the crack tip. The front of the specimens received a DIC spackle pattern that had a sigma level equal or below 0.001 [13]. The sigma level was tested during the baseline measurements stages until the desired value was achieved. The baseline measurements also utilized DIC to gather initial measurement errors bounds; if the load frame indicated a 0.2 mm displacement, did the DIC measurements also show a similar value? This was done by only pining the stationary end of the specimen and comparing the displacement between the load frame and DIC calculations. Additional baseline measurements included static DIC measurements at 0, 200, 1100, and 2000 N, as well as microscope crack measurements at no load and 2000 N. The initial crack growth was a step used to develop a crack and go outside the envelope of the stress-strain effects of the notch radius [15]. The notch radius was 0.17 mm, and an initial starter crack was developed to be around 1 mm in length. The HF pulse was applied at about 40 K cycles when the desired crack length was reached; subsequent measurements monitored the crack growth rates after the HF pulse was applied to evaluate the recovery. It is important to note that the load ranged from 200 N to 2000 N, where the stress ratio R = 0.1, the frequency used for fatigue was 5 Hz, and the nominal stress intensity $\Delta K = 6.07$ MPa-m$^{0.5}$.

The experimental matrix utilized is shown in Table 2.1; it consists of a baseline test where no HF pulse is applied, and a 3×3 matrix with three levels and two factors (amplitude, frequency), resulting in 9 treatments, where the amplitude of the pulse is increased in 1/3 amplitude increments and frequencies that range between 4 and 10 times the baseline frequency, i.e., specimen 3C had a peak amplitude of 2900 N and an HF pulse with a frequency of 50 Hz.
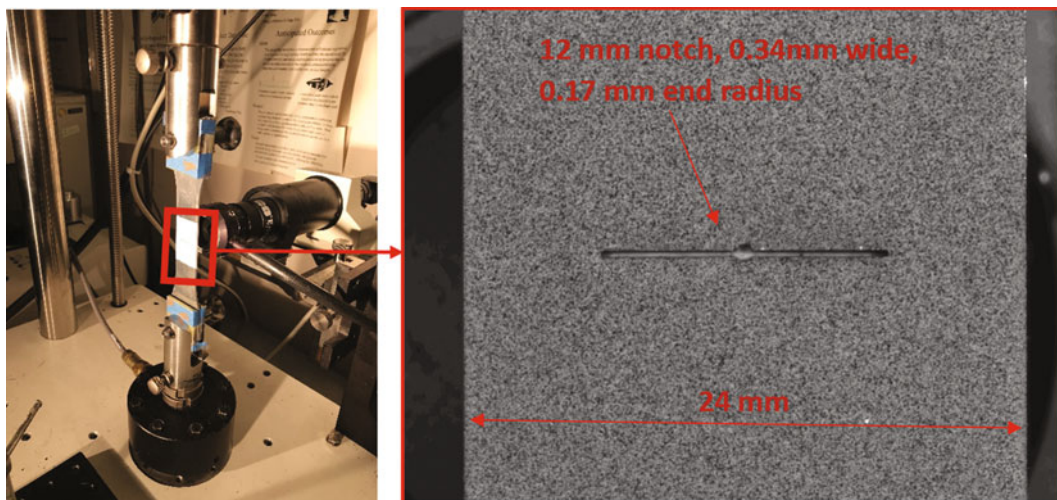

Fig. 2.5 Specimen and speckle pattern

Fig. 2.6 Experimental process

Table 2.1 Test matrix for HF pulse loading conditions

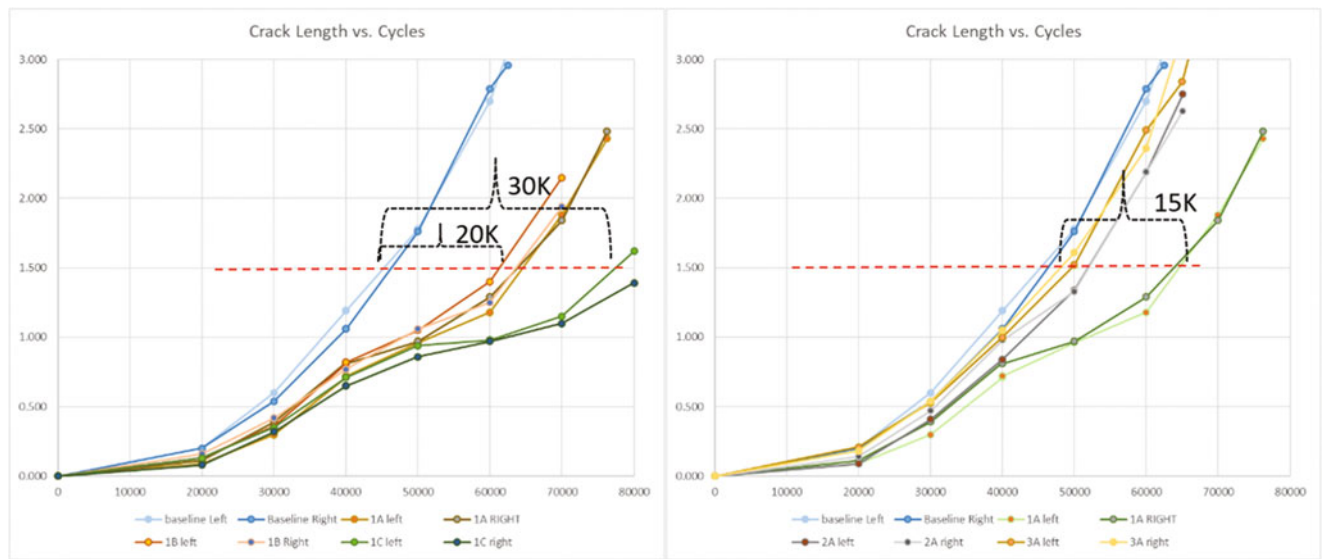|		High Frequency Pulse Amplitude (N)		
	Baseline, No Effects	1/3 Peak Amplitude	2/3 Peak Amplitude	Peak Amplitude
		2300	2600	2900
High Frequency Pulse Frequency (Hz)	4 x Main Wave 20	1A	1B	1C
	7 x Main Wave 35	2A	2B	2C
	10 x Main Wave 50	3A	3B	3C

Fig. 2.7 Crack length for varying load (left) and frequency (Right)

For this matrix, the HF pulse was only applied at the peak of the ordinary wave of 5 Hz; hence the phase shift was held constant as well as the log decrement of the function was maintained at 0.21. Introduction of other factors would increase the matrix size to a 3^3 design resulting in 27 treatments and are recommended for future experiments.

2.4 Experimental Results

When plotting the data, as shown in Fig. 2.7, the initial results were the crack length for specimens where the load is varied while the frequency is held constant (left) and specimens where the frequency is held constant and the load is varied (right). One can see that when comparing the number of cycles it takes to grow a crack to a nominal length of 1.5 mm, the varying load (left) has a noticeable effect on the crack growth. It takes 20–30 K cycles in delay depending on the load. One can see that the number of cycles it takes for the crack to grow 0.5 mm on the baseline is substantially smaller that the cycles needed for the specimens that had an HF pulse applied. When looking at the varying frequency (right), one can see that a lower frequency has a higher effect for the same max load of 2300 N. When looking diagonally across the matrix, one can see in Fig. 2.7 that the lowest block with the lowest load and frequency behaves very similarly to the baseline, but other blocks begin to deviate as the load and frequency of the HF pulse are increased.

Vic2D DIC was utilized to evaluate the strain fields ahead of the crack before and after the HF pulse was applied. Figure 2.8 shows the various stages of the strain changes surrounding the crack; in addition, the complete crack path is also shown in relation to the strain zones. At 40 K cycles, the crack is moving in a downward direction, and upon application of the HF
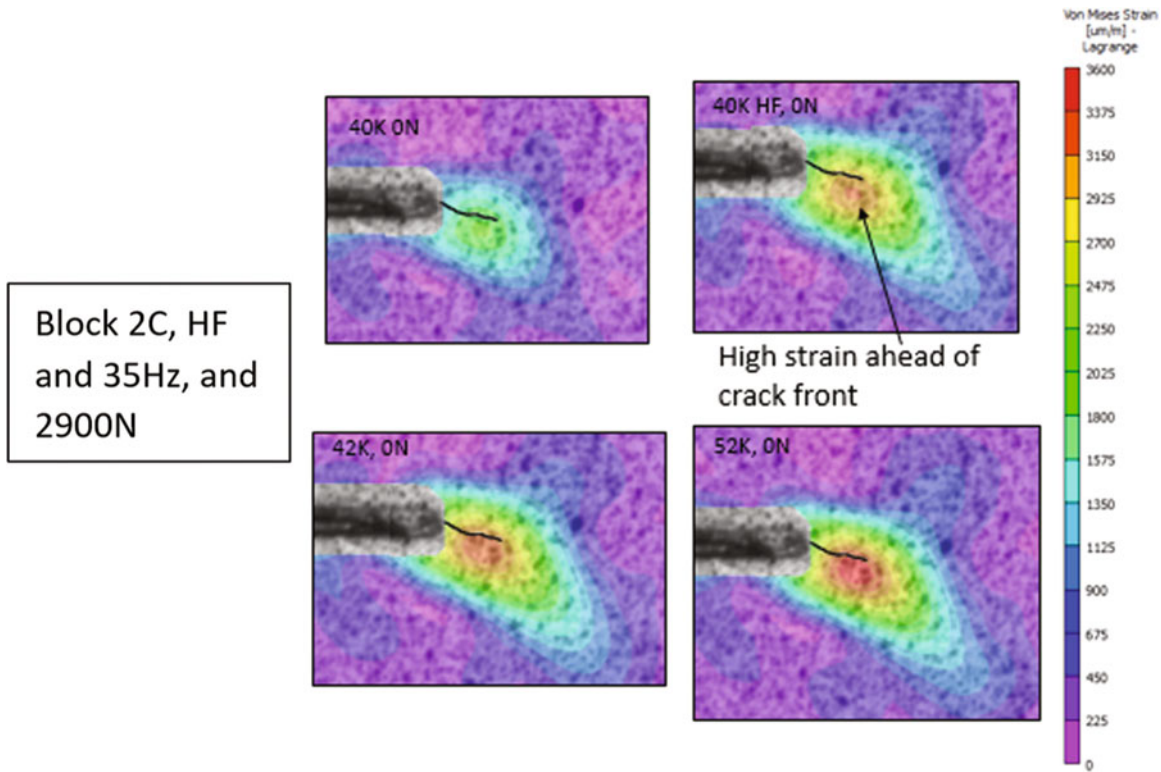
Fig. 2.8 Strain field evolution, block 2C at HF of 35 Hz, and peak amplitude of 2600 N

Wheeler

$$\frac{da}{dN} = \Phi_R \left(\frac{da}{dN}\right)_{CAL}$$

$$\text{where}: \Phi_R = \begin{cases} \left[\frac{r_{p,i}}{a_{OL} + r_{p,OL} - a_i}\right]^m & \text{when} \quad a_i + r_{p,i} < a_{OL} + r_{p,OL} \\ 1 & \text{when} \quad a_i + r_{p,i} > a_{OL} + r_{p,OL} \end{cases}$$

Willenborg

$$\frac{da}{dN_i} = \frac{C(\Delta K_{eff})_i^m}{[(1 - R_{eff})_i]K_c - (\Delta K_{eff})_i}$$

Fig. 2.9 Wheeler and Willenborg models

pulse, a high strain hardening region is developed ahead of the crack, acting like a hard inclusion. The DIC data show how strains changed from 42 K cycles to 52 K cycles, including its size and dimensions; it includes utilization of work by Bruck [16], and modification work by Yates was utilized to locate the crack tip location [17] and associated plastic zone [18, 19]. The DIC data capture a kinking of the crack, also observed in microscope measurements, and how it circumvents around this are of high strain in order to continue its growth. This highlighted future work needed in investigating the strain fields ahead of the crack and shear effects to better understand the kinking behavior. This all leads to gaining a deeper understanding of the behavior observed by Laseure [7].

At the core of this work are the models by heeler [4] and Willenborg [5]. These models look at the plastic zone behavior, Wheeler relies on crack growth rates, and Willenborg utilizes stress intensity for the calculation, as shown in (Fig. 2.9):

More recent research work by Mehrzadi and Taheri [6] and Chen [19] outline the behavior of the plastic zone ahead of the crack tip. The common thread of all these models is that an overload plastic zone is created once an overload/underload occurs, and the magnitude of this region has an effect on the crack growth rate as long as the cyclic plastic zone stays within its boundaries. The radii of the plastic and overload zone can be calculated utilizing the Irwin approximation [20]. The
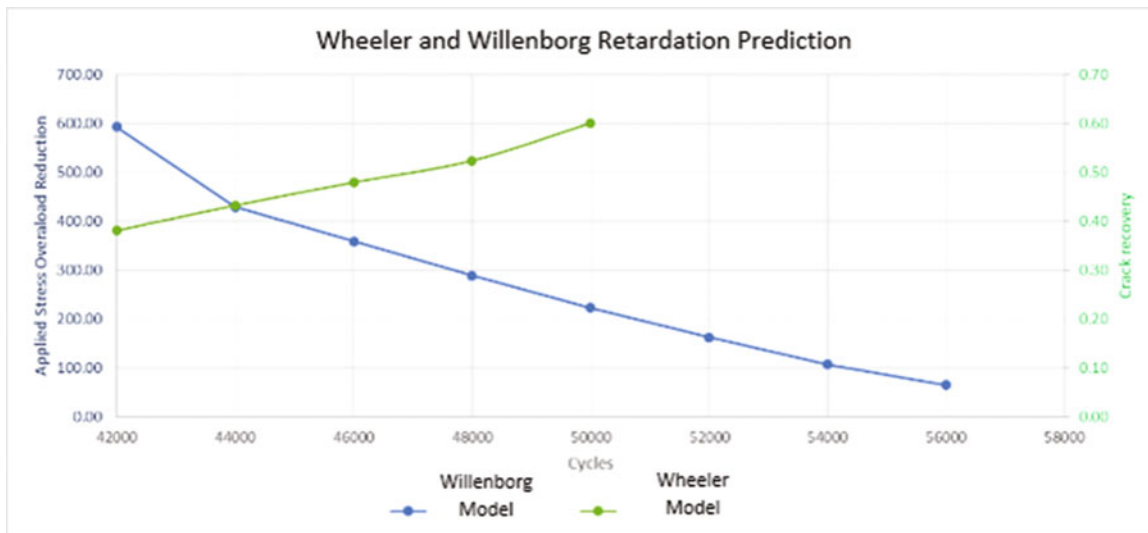
Fig. 2.10 Wheeler and Willenborg retardation predictions of HF pulse of 50 Hz and 2900 N

Wheeler model relies on the Irwin calculation to develop the radii of the overload zone and cyclic zones. The methodology of the Wheler model is that an overload plastic zone is created and retardation occurs as long as the reoccurring cyclic zone is within the bounds of the overload zone as the crack grows. The Willenborg model follows a very similar approach but relies on the stress intensity from the overload [15] and the calculation of a stress intensity reduction in order for retardation effects to seize. This behavior can be seen graphically showing how the residual stress intensity is accumulated after the HF pulse at 42 K cycles and how it diminishes over time to no retardation at 56 K cycles for the Willenborg model, Fig. 2.10. For the Wheeler model, the crack recovery can also be plotted to show when the radii of the cyclic plastic zone reaches the boundary of the overload zone and also hence ends the retardation cycle at 50 K cycles.

One of the novel findings of this work was the observation of a crack kinking mechanism resulting from the application of certain HF pulses, outlined in the next section.

2.5 Crack Kinking Behavior

An observed crack kinking behavior was mentioned in previous sections, during the experiments; this behavior was observed and tracked for the various specimen conditions outlined in Table 2.1. The microscope data shown in Fig. 2.11 show the crack growing from the left notch of each specimen, the orange arrow marks the direction of crack growth, the red mark shows the application of the applicable HF pulse, the green marks delimitate locations of data extraction in the fatigue cycle.

While the microscope measurements provide a view of the crack propagation, a Barker's etch method [21] was used for anodizing the aluminum alloy and then utilizing optical microscopy with polarized lights to observe the grain boundary and the propagated crack. This was evaluated at 500 µm, 100 µm, and 20 µm magnification levels, allowing the evaluation of the crack propagation through the grain, evaluating if there was a presence of large material inclusions, as well as investigating shielding effects such as contact and deflection on crack growth [22]. Fractography was also utilized to examine the surfaces through the crack depth on the specimen; several test specimens were carefully cut to allow views of the through thickness crack front. The results showed a distinct beach mark shape due to the HF pulse and a change in contrast near the edge surfaces due to the inclination associated with crack kinking. This evaluation also showed that the width of the beach mark is consistent with plastic zone and narrows beneath the surface as it is typical of plane stress to plane strain transition regions. This assessment did not indicate that there was a presence of a material inclusion that could cause the observed kinking behavior.

The crack kinking behavior observed can be segmented into several areas associated with the kinking condition, as shown in Fig. 2.12. After the application of the HF pulse, there is a section when the crack continues to grow, and before it kinks, another section is when the crack is fully kinked and continues in that condition, and a last section where the crack kinking behavior has ceased and the crack has returned to its semi-original growth path. Length and angle parameters were gathered for the crack.L1 defines the crack length after the HF pulse and before the kink, L2 defines the length of the kink. The angle
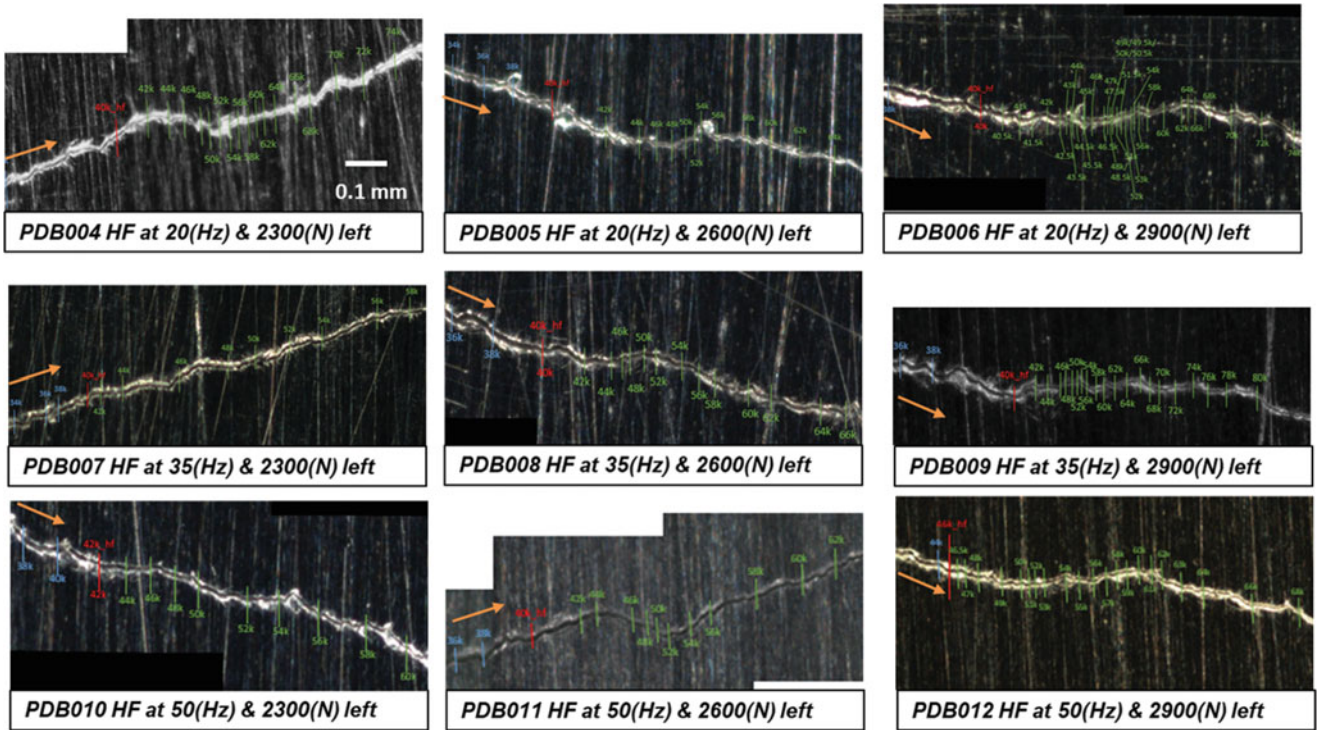
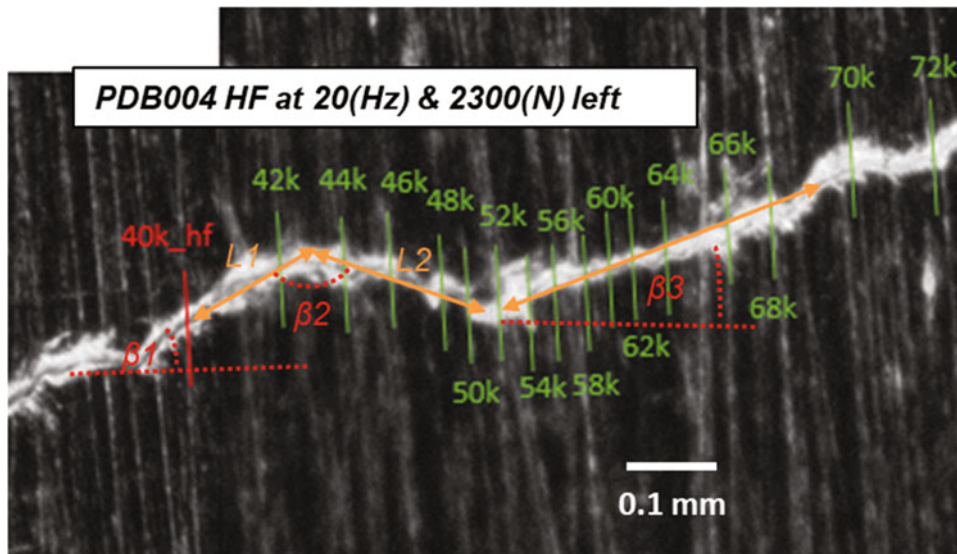**Fig. 2.11** Crack kinking behavior matrix

Fig. 2.12 Crack kinking characterization

β1 defined the entry angle in relation to the horizontal plane, β2 is the kink angle between L1 and L2, and β3 is the exit angle with respect to the horizontal.

It is worth noting that the entry angle β1 is dependent on the original direction of crack growth and independent of the HF pulse condition, as specimens do not have a consistent entry angle β1 of crack growth, which can be dependent on notch conditions and presence of inclusions during initial crack growth. The crack kink data highlighted several findings; one was that the kink angle β2 is consistent between experiments and has a mean of 136 degrees as measured between L1 and L2. Another finding was that the exit angle β3 is consistently less than the entry angle β1 by a mean of 2 degrees.

2.6 Effects of HF Pulse on Da/DN

The data also allowed for the identification of the variation of Da/DN, as shown in Fig. 2.2, but with higher fidelity to who show the effects of an application of the HF pulse. In Fig. 2.13, the left figure shows that retardation effects are quite consistent over several test specimens that received the same HF pulse, but these effects are not quite present as shown on the right figure, where the HF pulse increased in frequency to 50 Hz, but maintained a maximum load of 2300 N. This observation can also be seen on Fig. 2.11, where no kinking is observed for the specimen on the lower left quadrant.

While the results do not show a very clear crack retardation from certain HF pulses, it does provide data to show that the experimental matrix was able to capture limitations toward the presence of kinking behavior, where certain loading conditions do not precipitate a clear kinking of the crack, but instead less visible retardation effect. By leveraging the characterization of the crack kinking, as shown in Fig. 2.12, it is possible to examine the crack growth rate for varying frequency and load. Figure 2.14 shows these values and certain observations can be gathered from the results. The behavior of increased crack growth rate after the HF pulse and decrease during the kink portion can be observed. Another observation is that by varying the HF pulse form 2300–2900 N and maintaining a frequency of 20 Hz, affects the Da/DN after the HF pulse, but also reduces Da/DN during the kinking portion of the crack growth.

However, by holding the load constant at 2900 N and increasing frequency, the Da/DN during the kink actually increases. This data was very promising as it shows The DIC data allows for the interrogation of surface strains ahead of the crack path
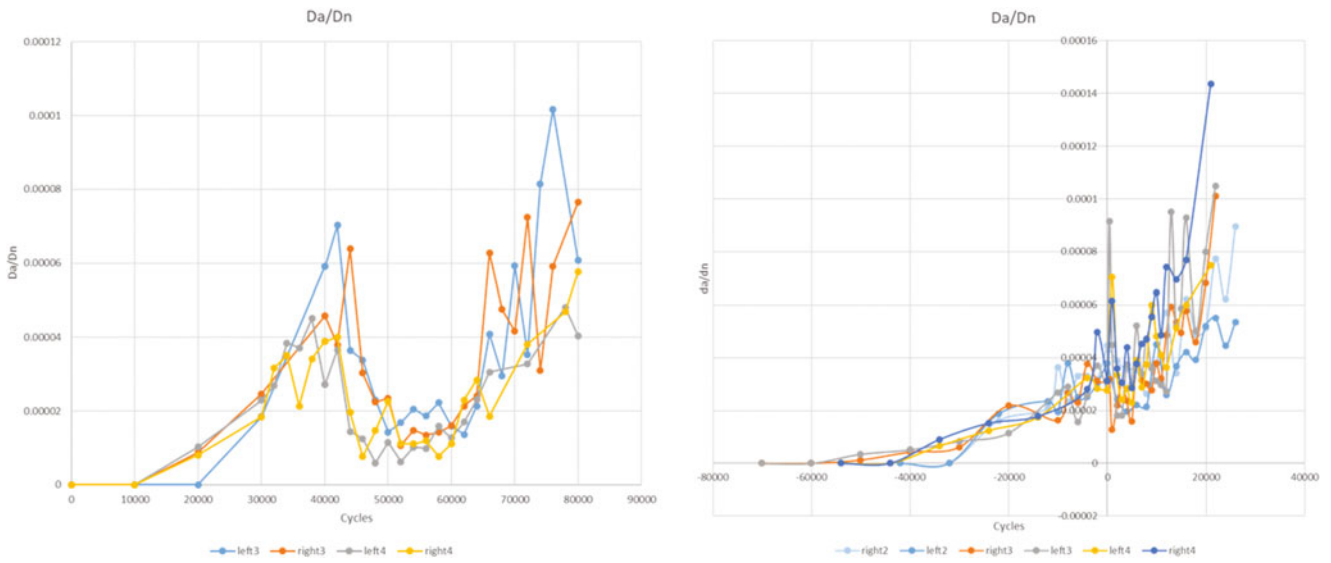

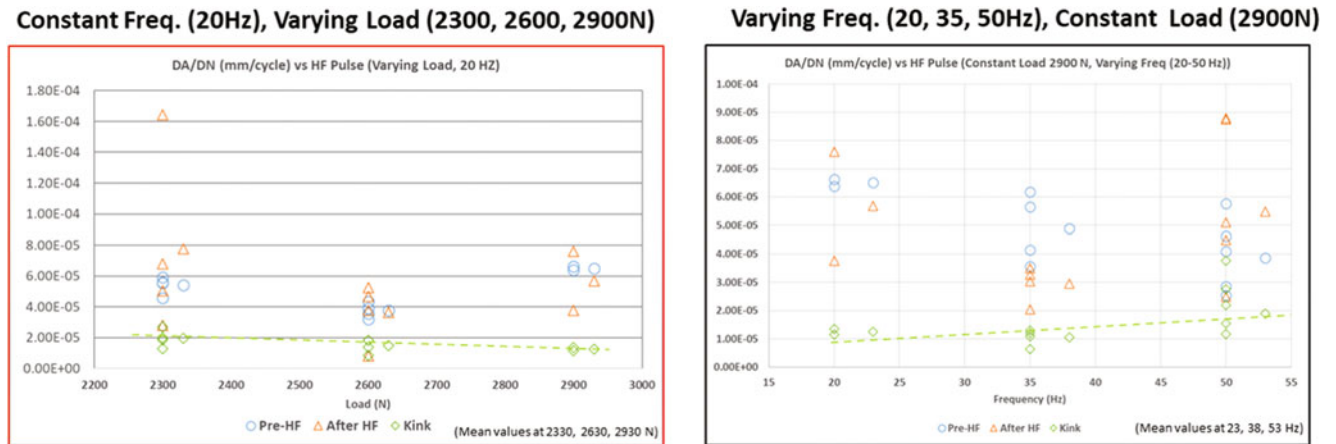**Fig. 2.13** HF pulse applied at 20 Hz and 2300 N (left) and 50 Hz and 2300 N (right)

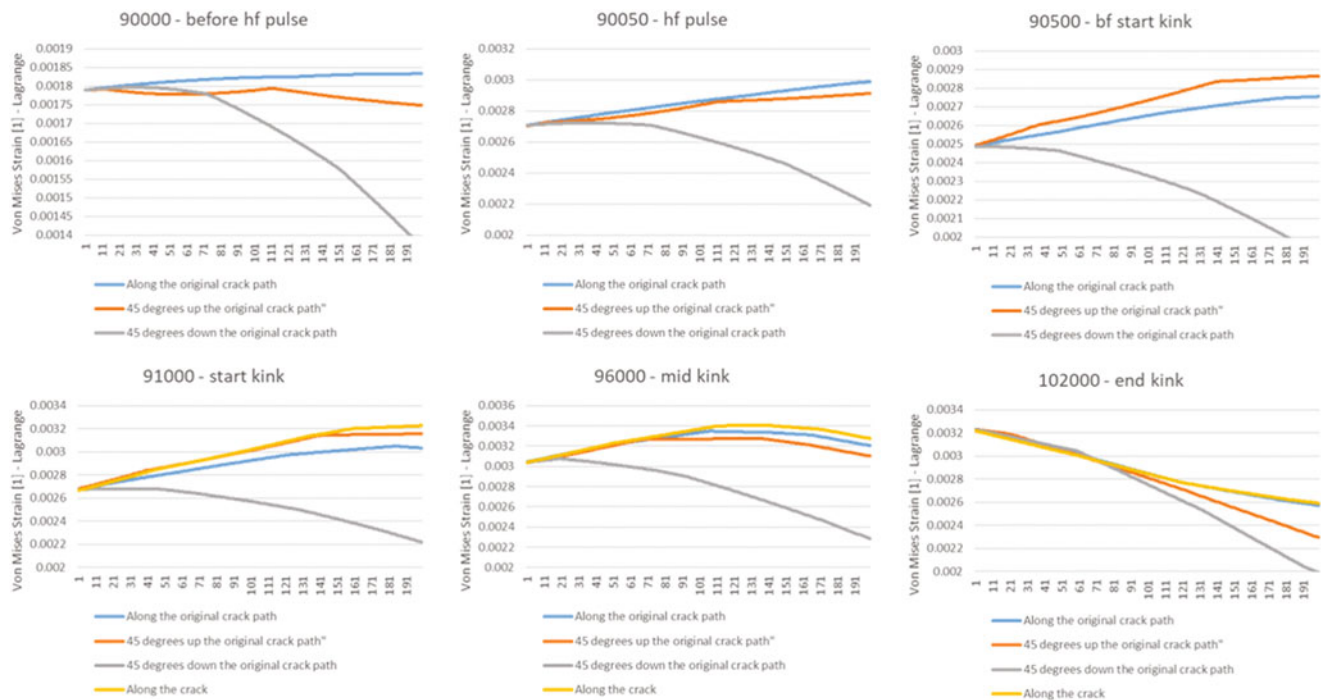**Fig. 2.14** Da/DN, variation of load and frequency

Fig. 2.15 Von Mises strain fields ahead of crack

along different vectors, and to see how they evolve over time. Figure 2.15 shows these Von Mises strain fields at ±45° from the crack direction, as well as along original crack path. That the matrix captures a variation of crack growth rates, as well as kinking behavior which is affected by both magnitude and frequency.

The fanning of the strain fields changes due to the application of the HF pulses and has a very distinctive variability when the kink is complete.

Work is ongoing to utilize DIC strain and crack opening displacement (COD) to develop a flow model that steps through different conditions that would trigger kinking effects and their termination. As initially expected, DIC data are providing critical data in understanding how the surface strains vary and their correlation to the effects of HF pulses.

2.7 Conclusions

Existing models like the Wheeler, Willenborg, and variations of these have been utilized to predict the crack growth behavior with varying degrees of success. In this work, we carried through an experimental matrix to explore the effects of HF pulses on fatigue crack growth in 5xxx aluminum, typically used in marine applications. We utilized visual inspection of crack tip location and used digital image correlation (DIC) techniques for characterization of the crack tip deformation fields. These techniques were used on a designed center crack tension (CCT) panel specimens to measure crack growth. DIC techniques also enabled additional analysis of strain fields to better understand the associated crack growth behavior. A novel crack kinking behavior was observed from certain HF pulses; this kinking behavior was characterized and several metrics were extracted to show its influence on crack growth rates and retardation. This ongoing work includes utilizing this observed data to finalize an embedded high frequency load models for fatigue crack growth and exploring the phasing of HF pulses.

2.8 Future Work

This experimental data is providing basin information toward the kinking behavior and crack retardation from the application of HF pulses, but it also highlights areas where additional work is needed. There are long-term efforts and shorter-term actions on this. Long term there is the evaluation of heat-affected zones and weld effects, introduction of other materials, and

expansion to include other variables such as HF pulse shift or decay rates. Short-term actions aim to target some particular critical efforts in gaining a deeper understanding of this behavior. This includes work in relation to the sequencing of HF pulses to gain understanding on the effects of kinking and delay.

References

1. Murthy, R., Palani, G., Iyer, N.: State-of-the-art review on fatigue crack growth analysis under variable amplitude loading. IE(I) J., 12 (2004)
2. Sumi, Y.: Fatigue crack propagation in marine structures under seaway loading. Int. J. Fatigue, 7 (2014)
3. Fricke, W., Paetzold, H.: Experimental Investigations on Fatigue Damage of Ship Structures Caused by Whipping Stresses. In: PRADS, Changwon City, Korea (2013)
4. Wheeler, O.: Spectrum loading and crack growth. J. Basic Eng. Transport. ASME, 5 (1972)
5. Willenborg, J., Engle, R., Wood, H.: A crack growth retardation model using an effective stress concept. AFFDL TM-71-1-FBR, Jan 1971 (1971)
6. Mehrzadi, M., Taheri, F.: A material sensitive modified wheeler model for predicting the retardation in fatigue response of AM60B due to an overload. Int. J. Fatigue, 10 (2013)
7. Laseure, N.S.I.M.N.D.W.W.: Effects of Variable Amplitude Loading on Fatigue Life. Ghent University, Labo Soete, Ghent (2016)
8. Hart, D., Bruck, H.: Characterization and modeling of low Modulus composite patched center crack tension specimen using DIC surface. In: Society of Experimental Mechanics (2018)
9. ASTM-E8: ASTM E8M-08: Standard Test Methods for Tension Testing of Metallic Materials. ASTM International, Conshohocken (2008)
10. ASTM-E466: ASTM E466–07: Standard Practice for Conducting Force Controlled Constant Amplitude Axial Fatigue Tests of Metallic Materials. ASTM International, Conshohocken (2007)
11. ASTM-E647: Standard Test Method for Measuring Fatigue Crack Growth Rates. ASTM International, Conshohocken (2015)
12. ASTM-E338: Standard Test Method of Sharp-Notch Tension Testing of High-Strength Sheet Materials. ASTM International, Conshohocken (2003)
13. Sutton, M., Orteu, J.-J., Schreier, H.: Image Correlation for Shape, Motion, and Deformation Measurements. Springer LLC, Boston (2009)
14. Jones, E.: Good practices guide for digital image Correllation. Int. Digital Image Correl. Soc. (2018)
15. Bannantine, J., Comer, J., Handrock, J.: Fundamentals of Metal Fatigue Analysis. Prentice Hall Inc, Upper Saddle River (1990)
16. Bruck, H.: Analysis of 3-D Effects near the Crack Tip on Rice's 2-D J-Integral Using Digital Image Correllation and Smoothing Techniques, M.S. Thesis, Univeristy of South Carolina (1989)
17. Yates, J., Zanganeh, Y.: Quantifying crack tip displacement fields with DIC. Eng. Fracture Mech., 14 (2010)
18. Gdoutos, E.: Fracture Mechanics, An Introduction, 2nd edn. Springer, Minneapolis (2005)
19. Chen, F., Wang, F., Cui, W.: Fatigue life prediction of engineering structures subjected to variable amplitude loading using the improved crack growth rate model. Fatigue Fracture Eng. Mater. Struct., 13 (2011)
20. Anderson, T.: Fracture Mechanics Fundamental and Applications, 3rd edn. Taylor and Francis Group LLC, Boca Raton (2005)
21. Cerri, E., Evangelista, E.: Metallography of Aluminum Alloys. Mechanical Engineering Department, European Aluminum Association, Ancona (1999)
22. Ritchie, R.: Mechanisms of fatigue crack propagation in metals, ceramics and composites: role of crack tip shielding. Mater. Sci. Eng. **A103**, 14 (1988)